Frequency Invariant Uniform Concentric Circular Arrays with Directional Elements

BIN LIAO, Student Member, IEEE
KAI-MAN TSUI
SHING-CHOW CHAN, Member, IEEE
The University of Hong Kong

A new approach for designing frequency invariant (FI) uniform concentric circular arrays (UCCAs) with directional elements is proposed, and their applications to direction-of-arrival (DOA) estimation and adaptive beamforming are studied. By treating the sensors along the radial direction of the UCCA as linear subarrays and using appropriately designed beamformers, each subarray is transformed to a virtual element with appropriate directivity. Consequently, the whole UCCA can be viewed as a virtual uniform circular array (UCA) with desired element directivity for broadband processing. By extending the approach for designing FI-UCAs, the frequency dependency of the phase modes of the virtual UCA is compensated to facilitate broadband DOA and adaptive beamforming. Both the linear array beamformers (LABFs) and compensation filters can be designed separately using second-order cone programming (SOCP). Moreover, a new method to tackle the possible noise amplification problem in such large arrays by imposing additional norm constraints on the design of the compensation filters is proposed. The advantages of this decoupled approach are 1) the complicated design problem of large UCCAs can be decoupled into simpler problems of designing the LABFs and compensation filters, and 2) directional elements, which are frequently encountered, can be treated readily under the proposed framework. Numerical examples are provided to demonstrate the effectiveness and improvement of the proposed methods in DOA estimation, adaptive beamforming, and elevation control over the conventional FI-UCCA design method.

Manuscript received August 19, 2011; revised February 7, 2012; released for publication July 7, 2012.

IEEE Log No. T-AES/49/2/944506.

Refereeing of this contribution was handled by W. Blanding.

Authors' address: Department of Electrical and Electronic Engineering, The University of Hong Kong, Pok Fu Lam Road, Hong Kong, E-mail: (scchan@eee.hku.hk).

I. INTRODUCTION

Broadband beamforming has been successfully applied to many fields, including wireless communications, radar, radio astronomy, sonar, navigation, tracking, rescue, and other emergency-assistance devices. Hence, the theoretical as well as applied aspects of broadband beamforming have received great research interest during the last decades [1, 2]. One of the most popular approaches for adaptive broadband beamforming is to employ tapped-delay lines or linear transversal filters with adaptive coefficients to generate appropriate beampatterns for the suppression of undesirable interference. Since the response of the array is frequency dependent, the number of coefficients of the tapped-delay lines required will increase with the signal bandwidth, which implies high complexity for broadband adaptive processing. To tackle this problem the subband decomposition technique, partial adaptation, and frequency invariant beamformers (FIBs) have been proposed to reduce either the frequency band to be adapted or the length of the adaptive transversal filters [3–10] to be employed.

In FIB a fixed beamforming network is used to compensate for the frequency dependency of the array and to achieve beampatterns which are approximately invariant over the frequency band of interest. For instance, in [6], the array aperture is discretized to obtain FIBs with fixed beampatterns using the scale-frequency relationship of an array aperture. The design and implementation of such FIBs for linear arrays have been reported in [7], and its application to direction-of-arrival (DOA) estimation using a beam-space processing approach has been studied in [8]. Because of the discretization process, the positions of the sensor elements are usually nonuniform. In [9] and [10] it is observed that the design of FIBs for uniform linear arrays (ULAs) is equivalent to the design of a 2D fan filter with different orientations. By using a set of fixed FIBs that covers different spatial angles of a ULA, broadband interferences can be suppressed using conventional beamforming methods. Most of the abovementioned works focus on linear arrays.

On the other hand it is known that circular arrays possess important advantages such as electronic steering and broadband processing, including beamforming and DOA estimation, etc. In [11] an electronic steerable uniform circular array (UCA) in the digital domain with approximately frequency invariant (FI) characteristics was proposed. Compensation filters, which can be optimally designed using second-order cone programming (SOCP), were introduced to suppress the frequency variations. The possibility of using compensation filters in UCAs has also been experimentally demonstrated for sonar applications in [12]. More recently uniform concentric

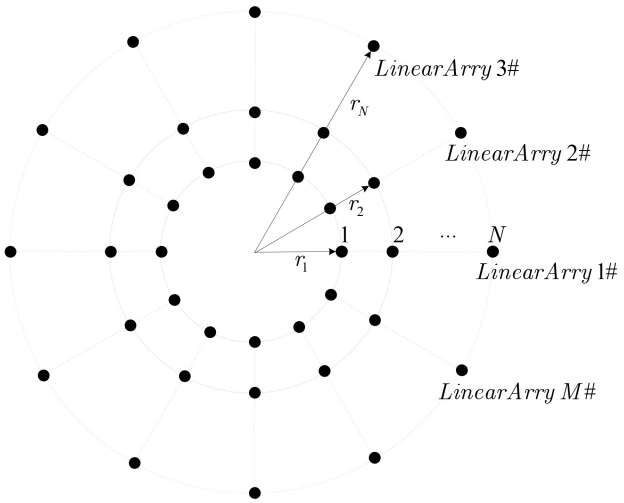

Fig. 1. UCCA composed of M linear arrays, each with N elements.

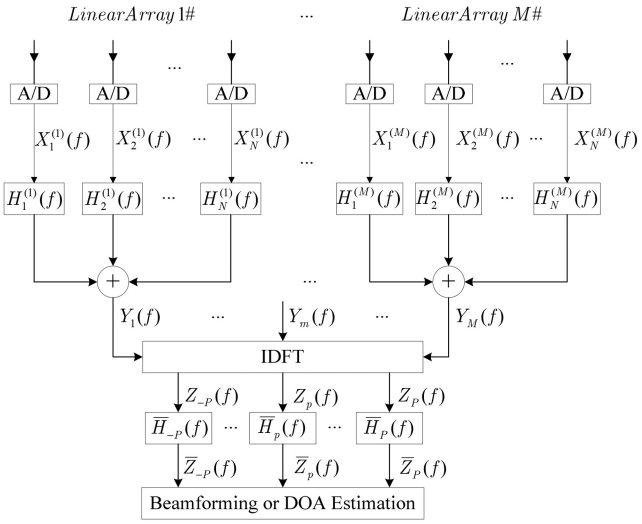

Fig. 2. Block diagram of proposed UCCA-FIB.

circular arrays (UCCA) were extensively studied in [13]–[15] and the related references therein. It is found that FI characteristics over a much larger bandwidth can be achieved by using UCCAs instead of UCAs for omnidirectional sensors.

It is worth noting that the methods mentioned above are usually based on omnidirectional elements [16–18]. Motivated by the important advantages of UCCAs and by the directivity of the sensor elements commonly encountered in circular arrays, we propose, in this paper, a new approach to the design of FI-UCCAs with directional elements, as shown in Figs. 1 and 2. More specifically we treat the sensors along the radial direction on the sensor plane as linear subarrays. Each subarray is transformed to a virtual element with appropriate directivity by means of an appropriately designed linear array beamformer (LABF). Consequently, the whole UCCA can now be viewed as a virtual UCA with suitable element directivity for broadband processing. By extending the approach in [17], the frequency dependency of the phase modes of the virtual UCA, which are the inverse discrete Fourier transform (IDFT) of the subarray outputs, is compensated in order to facilitate broadband DOA and adaptive beamforming. Both the LABFs and compensation filters can be designed separately using SOCP, which can be efficiently and optimally solved. The advantages of this approach are 1) the complicated design problem of a UCCA can now be decoupled into the simpler problems of designing the LABFs and compensation filters for the UCA, and 2) directional elements, which are frequently encountered, can be treated readily under the proposed framework. In particular it is simpler to determine the locations of the sensors than a general UCCA with a lot of sensors. This simplicity, however, will also impose some limitations to the ultimate performance of the array as a tradeoff.

In the design of a UCCA with a large number of elements and wide bandwidth, the beamforming network or compensation filters may lead to coefficients with large amplitude and, hence, sensor noise amplification. To address this problem we propose imposing additional norm constraints on the filter coefficients so as to restrict the amplitude of the filter coefficients and, hence, possible sensor noise amplification. The resultant problem can also be solved using the SOCP.

Moreover, the proposed UCCA-FIB is exploited for broadband DOA estimation and adaptive beamforming. Different from most traditional FIB-based DOA methods, which usually require additional beam-space processing, we propose applying directly conventional narrowband methods for ULAs such as MUSIC [19] to phase modes since the steering vector of our virtual FI-UCA has the same form as a narrowband ULA. This considerably simplifies the implementation and allows other, more-sophisticated methods that have been developed for ULAs to be applied. With the incorporation of norm constraints, it is found from simulation results that the proposed constrained UCCA-FIB offers satisfactory performance for both DOA and adaptive beamforming with very few variable beamformer weights and simple operation.

The rest of the paper is organized as follows. In Section II the basic structure of the UCCA with directional elements and the proposed digital broadband UCCA-FIB are presented. The design of the compensation filters for the FIB is described in Section III. Section IV is devoted to the extension of the proposed UCCA-FIB with elevation beampattern control. The proposed broadband DOA estimation and adaptive beamforming algorithms that use the proposed UCCA-FIB are presented in Section V. Design examples are given in Section VI to illustrate

the effectiveness of the proposed method. Finally, Section VI concludes the paper.

II. DESIGN OF FIB FOR UCCA

The UCCA studied in this paper is shown in Fig. 1. It is assumed that the UCCA is composed of N rings, each of which is a UCA with M sensor elements. Alternatively, the UCCA can also be viewed as an $M-$element UCA with each sensor element consisting of a linear array, each with N sensor elements. Therefore, the steering vector of the mth linear array can be given by

$$\begin{aligned}\mathbf{a}^{(m)}(f,\theta,\phi) &= \{E_1^{(m)}(\theta,\phi-\varphi_m)\exp[j\beta r_1\sin\theta\cos(\phi-\varphi_m)],\\ &\quad E_2^{(m)}(\theta,\phi-\varphi_m)\exp[j\beta r_2\sin\theta\cos(\phi-\varphi_m)],\ldots,\\ &\quad E_N^{(m)}(\theta,\phi-\varphi_m)\exp[j\beta r_N\sin\theta\cos(\phi-\varphi_m)]\}^T\end{aligned}$$

where $\beta = 2\pi f/c$, $f \in [f_L, f_U]$ is the frequency within the desired range, c is the propagation velocity, and r_n denotes the radius of the nth ring. θ and ϕ are the elevation angle and azimuth angle, respectively. $\varphi_m = 2\pi(m-1)/M$ represents the angular position of the mth linear array. $E_n^{(m)}(\theta,\phi)$ is the element pattern of the nth element in the mth linear array. In particular, $E_n^{(m)}(\theta,\phi) = 1$ denotes an omnidirectional element. In this paper we mainly focus on the design at the elevation angle of $\theta = \pi/2$, i.e., the horizontal plane. However, we later show that a limited range of the elevation spatial pattern around the horizontal plane can also be controlled by using the proposed method.

Figure 2 shows the structure of the proposed FIB for UCCAs. The basic principle is to transform each linear subarray of the UCCA to an equivalent element with an appropriate directional pattern. Consequently, a virtual UCA consisting of these desirable directional elements with a radius of r_V is obtained. Let $x_n^{(m)}[t,\phi]$ be the output of the nth element of the mth linear array. It is first passed through a filter $h_n^{(m)}[t]$ with frequency response $H_n^{(m)}(f)$. Then, all filter outputs are summed to give the output of each linear subarray as

$$y_m[t,\phi] = \sum_{n=1}^{N} x_n^{(m)}[t,\phi] * h_n^{(m)}[t] \tag{1}$$

where $*$ denotes discrete-time convolution. The filters $H_n^{(m)}(f)$, $n = 1,\ldots,N$, form the LABF of the mth linear subarray. By applying the discrete-time Fourier transform (DTFT) to (1), one gets the spectrum of $y_m[t,\phi]$ as

$$Y_m(f,\phi) = \sum_{n=1}^{N} X_n^{(m)}(f,\phi)H_n^{(m)}(f) \tag{2}$$

where $X_n^{(m)}(f,\phi)$ and $H_n^{(m)}(f)$ are the DTFT of $x_n^{(m)}[t,\phi]$ and $h_n^{(m)}[t]$, respectively.

Assuming that the source $s[t]$ with spectrum $S(f)$ impinges on the array from angle ϕ, we then have $X_n^{(m)}(f,\phi) = S(f)E_n^{(m)}(\phi-\varphi_m)\exp[j\beta r_n\cos(\phi-\varphi_m)]$. By substituting this back into (2), one gets

$$Y_m(f,\phi) = S(f)G_m(f,\phi) \tag{3a}$$

where

$$G_m(f,\phi) = \sum_{n=1}^{N} E_n^{(m)}(\phi-\varphi_m)\exp[j\beta r_n\cos(\phi-\varphi_m)]H_n^{(m)}(f) \tag{3b}$$

is the spatial response of the mth linear array. Alternatively, the UCCA can now be viewed as a UCA with directional elements having an element response of $G_m(f,\phi)$. As pointed out in [17], a UCA with suitable directional elements can effectively synthesize wide-bandwidth array patterns. We discuss the choice of this element pattern for the proposed virtual UCA later in this section. If the LABFs $H_n^{(m)}(f)$ are designed so that each linear subarray behaves like a directional element being placed at a UCA with radius r_V, then it is possible to synthesize an FI wideband UCA. In other words we wish the mth linear array response $G_m(f,\phi)$ in (3b) to approximate the mth element response of a virtual UCA with radius r_V

$$G_m(f,\phi) \approx G(\phi-\varphi_m)\exp[j\beta r_V\cos(\phi-\varphi_m)] \tag{4}$$

where $G(\phi-\varphi_m)$ denotes the desired beampattern of the mth virtual element and r_V is chosen to lie in $[r_1, r_N]$. Consequently, the design of a UCCA with a large number of directional elements can be decoupled into the individual design of the LABF and an FI-UCA. For the latter we first note that the steering vector of the virtual UCA with M directional elements is given by

$$\begin{aligned}\mathbf{a}_V(f,\phi) = \{&G(\phi-\varphi_1)\exp[j\beta r_V\cos(\phi-\varphi_1)],\\ &G(\phi-\varphi_2)\exp[j\beta r_V\cos(\phi-\varphi_2)],\ldots,\\ &G(\phi-\varphi_M)\exp[j\beta r_V\cos(\phi-\varphi_M)]\}^T.\end{aligned}$$

One of the attractive features of circular arrays is that the directional pattern formed can be readily rotated in the azimuth direction without much variation by controlling the excitation or amplification of the phase modes. In fact, the design, analysis, and beamforming of UCA can be conveniently carried out by means of the phase mode [13–18], which can be obtained by taking the IDFT of each snapshot of the UCA to form a set of Fourier coefficients, each of which is called a phase mode. More precisely the pth-order phase mode of our ideal, virtual UCA, as given by the right hand side of (4), can be written as

$$\tilde{G}_p(f,\phi) = \frac{1}{M}\sum_{m=1}^{M} G(\phi-\varphi_m)\exp[j\beta r_V\cos(\phi-\varphi_m)]e^{jp\varphi_m} \tag{5}$$

where $p = -P,\ldots,P$, and hence, the number of phase modes is $2P+1$.

As mentioned earlier $G(\phi)$ is the desired element pattern of the virtual UCA, and it should be designed according to the specifications of the target applications. In the context of wideband FI beamforming, the choice of $G(\phi)$ would be crucial to the resulting performance of the virtual UCA. For example, if $G(\phi)$ is chosen to be omnidirectional, the amplitudes of the modes at some frequencies may vanish so that it would be difficult to compensate the frequency response over a large bandwidth by using the compensation filter $\bar{H}_p(f)$ at the next stage. An interesting element pattern $G(\phi)$ proposed in [17] is $1+\cos\phi$, which yields non-zero modes over a wide frequency range. Alternatively, one may use another form of $G(\phi)$, provided that it possesses a similar non-zero amplitude characteristic as $1+\cos\phi$. Since the pattern $G(\phi)=1+\cos\phi$ gives satisfactory performance, as demonstrated in Section VI, we focus on this pattern throughout this paper.

We now determine the condition of the FIB to achieve FI spatial beampatterns. First of all we note that the element pattern $G(\phi)$ of the virtual UCA is a periodic function with period 2π. Hence, it can be written in a Fourier series as

$$G(\phi)=\sum_{k=-K}^{K} C_k e^{jk\phi} \tag{6}$$

where C_k denotes the kth Fourier coefficient which can be computed as $C_k=(1/2\pi)\int_0^{2\pi} G(\phi)e^{-jk\phi}d\phi$. In principle, the value of K depends on the function $G(\phi)$, and it can be infinity. In practice, a sufficient number of terms are chosen to give a good approximation. For instance, $K=1$ when $G(\phi)$ is chosen as $1+\cos\phi$. By using the above property in (6), (5) can be further written as

$$\begin{aligned}\tilde{G}_p(f,\phi)&=\frac{1}{M}\sum_{m=1}^{M}\sum_{k=-K}^{K} C_l \exp[jk(\phi-\varphi_m)]\exp[j(\beta r_V\cos(\phi-\varphi_m)+p\varphi_m)]\\&=e^{jp\phi}\sum_{k=-K}^{K} C_k\left\{\frac{1}{M}\sum_{m=1}^{M}\exp[j((k-p)(\phi-\varphi_m)+\beta r_V\cos(\phi-\varphi_m))]\right\}.\end{aligned} \tag{7}$$

For sufficiently large values of M, the sum inside the square bracket of (7) can be approximated by an integral, as follows

$$\begin{aligned}&\frac{1}{M}\sum_{m=1}^{M}\exp[j((k-p)(\phi-\varphi_m)+\beta r_V\cos(\phi-\varphi_m))]\\&\quad\approx\frac{1}{2\pi}\int_0^{2\pi}\exp[j((k-p)(\phi-\varphi)+\beta r_V\cos(\phi-\varphi))]d\varphi\\&\quad=\frac{1}{2\pi}\int_0^{2\pi}\exp[j((p-k)(\varphi-\phi)+\beta r_V\cos(\varphi-\phi))]d(\varphi-\phi)\\&\quad=j^{p-k}J_{p-k}(\beta r_V)\end{aligned} \tag{8}$$

where $J_{p-k}(\beta r_V)$ is the Bessel function of the first kind of order $p-k$. Consequently, using (8), (7) can be simplified to

$$\tilde{G}_p(f,\phi)\approx B_p(f)e^{jp\phi} \tag{9}$$

where

$$B_p(f)=\sum_{k=-K}^{K} C_k j^{p-k}J_{p-k}(\beta r_V). \tag{10}$$

It can be seen from (9) that the phase mode is frequency dependent due to the presence of $B_p(f)$. Hence, to achieve a FI beampattern, each phase mode has to pass through an additional filter $\bar{H}_p(f)$, called the compensation filter, to remove this frequency dependency. Therefore, the ideal response of $\bar{H}_p(f)$ should satisfy

$$\bar{G}_p(f)=\tilde{G}_p(f)\bar{H}_p(f)=B_p(f)e^{jp\phi}\bar{H}_p(f)=e^{jp\phi} \tag{11}$$

or equivalently

$$\bar{H}_p(f)=B_p^{-1}(f). \tag{12}$$

After compensation the steering vector of the phase modes is now given by

$$\begin{aligned}\mathbf{a}_{PM}(\phi)&=[\bar{G}_{-P}(f),\bar{G}_{-(P-1)}(f),\ldots,\bar{G}_P(f)]^T\\&\approx[e^{-jP\phi},e^{-j(P-1)\phi},\ldots,e^{jP\phi}]^T.\end{aligned} \tag{13}$$

It can be seen that if the LABF and compensation filters are properly designed, then the steering vector is approximately FI. Furthermore, the above steering vector has the same form as a $(2P+1)-$element ULA. Consequently, all conventional DOA estimation and adaptive beamforming algorithms for ULAs can be seamlessly applied to provide the corresponding broadband processing using the proposed UCCA. For instance, let the beamforming weight vector be $\mathbf{w}=[w_{-P},w_{-(P-1)},\ldots,w_P]^T$, then the spatial response of the final beamformer is

$$F(\phi)\approx\mathbf{w}^T\mathbf{a}_{PM}(\phi)=\sum_{p=-P}^{P} w_p e^{jp\phi}. \tag{14}$$

This considerably simplifies broadband DOA estimation and adaptive beamforming as we illustrate further in Section V.

III. DESIGN OF LABFS AND COMPENSATION FILTERS FOR FIB

As mentioned in previous sections, the design of the proposed UCCA-FIB with directional elements can be decoupled into the design of LABFs

$\mathbf{H}_m(f) = [H_1^{(m)}(f),\ldots,H_N^{(m)}(f)]^T$ for constructing the virtual UCA and compensation filters $\bar{\mathbf{H}}(f) = [\bar{H}_{-P}(f),\ldots,\bar{H}_P(f)]^T$ for shaping the desired pattern using the directional elements. Both of which should be designed appropriately to give an FI characteristic in the frequency band of interest.

By extending the approach in [13], we now formulate these design problems as SOCP problems, which can be optimally solved. The main difference between the proposed approach and the one in [13] is that additional norm constraints on the filter coefficients are imposed since the sensor noise may be amplified by the filtering network in large UCCAs or broadband applications where coefficients with large amplitude will be encountered.

We first start with the design of the LABFs. The frequency response of the filter $H_n^{(m)}(f)$ is given by

$$H_n^{(m)}(f) = \sum_{l=1}^{L} h_{n,l}^{(m)} \exp[-j2\pi(l-1)f/f_s] \tag{15}$$

for $n = 1,\ldots,N$, where f_s denotes the sampling frequency, L is the number of taps, and $h_{n,l}^{(m)}$ is the lth impulse response coefficient of the nth filter. For simplicity, we assume that each filter $H_n^{(m)}(f)$ is composed of L taps. We know that the filters $\mathbf{H}_m(f) = [H_1^{(m)}(f),\ldots,H_N^{(m)}(f)]^T$ have to be chosen to satisfy the approximation in (4) $\forall\phi \in [-\pi,\pi]$ and $\forall f \in [f_L, f_U]$, where f_L and f_U are, respectively, the lower and the upper frequencies of interest. Hence, using (15), $G_m(f,\phi)$ can be rewritten as

$$\begin{aligned} G_m(f,\phi) = &\sum_{n=1}^{N}\sum_{l=1}^{L} h_{n,l}^{(m)} E_n^{(m)}(\phi-\varphi_m) \\ &\times \exp[j(\beta r_n \cos(\phi-\varphi_m) - 2\pi(l-1)f/f_s)] \end{aligned} \tag{16}$$

and its desired response is $G(\phi-\varphi_m)\exp[j\beta r_V \cdot\cos(\phi-\varphi_m)]$ as mentioned in (4). The filter coefficients $h_{n,l}^{(m)}$ can be determined by minimizing the L2 norm of the resultant approximation error. This can be formulated as the following optimization problem

$$\begin{aligned} \min_{h_{n,l}^{(m)}} \Bigg\| &\sum_{n=1}^{N}\sum_{l=1}^{L} h_{n,l}^{(m)} E_n^{(m)}(\phi-\varphi_m) \\ &\times \exp[j(\beta r_n \cos(\phi-\varphi_m) - 2\pi(l-1)f/f_s)] \\ &- G(\phi-\varphi_m)\exp[j\beta r_V \cos(\phi-\varphi_m)] \Bigg\|_2 \end{aligned} \tag{17}$$

for $\phi \in [-\pi,\pi]$, $f \in [f_L, f_U]$, which can be further rewritten in the following matrix form as

$$\begin{aligned} &\min_{\mathbf{h}_m,\varepsilon} \varepsilon \\ &\text{s.t.} \quad \|\mathbf{c}_m^T(f,\phi)\mathbf{h}_m - g_m(f,\phi)\|_2 \le \varepsilon \\ &\qquad \phi \in [-\pi,\pi], \quad f \in [f_L, f_U] \end{aligned} \tag{18}$$

where

$$\begin{aligned} \mathbf{h}_m &= [h_{1,1}^{(m)},\ldots,h_{1,L}^{(m)},h_{2,1}^{(m)},\ldots,h_{2,L}^{(m)},\ldots,h_{N,1}^{(m)},\ldots,h_{N,L}^{(m)}]^T \\ \mathbf{c}_m(f,\phi) &= [\bar{E}_{1,1}^{(m)},\ldots,\bar{E}_{1,L}^{(m)},\bar{E}_{2,1}^{(m)},\ldots,\bar{E}_{2,L}^{(m)},\ldots,\bar{E}_{N,1}^{(m)},\ldots,\bar{E}_{N,L}^{(m)}]^T \\ \bar{E}_{n,l}^{(m)} &= E_n^{(m)}(\phi-\varphi_m)\exp[j(\beta r_n\cos(\phi-\varphi_m) - 2\pi(l-1)f/f_s)] \\ g_m(f,\phi) &= G(\phi-\varphi_m)\exp[j\beta r_V\cos(\phi-\varphi_m)]. \end{aligned}$$

By discretizing the constraints densely in $f \in [f_L, f_U]$ and $\phi \in [-\pi,\pi]$, (18) can be expressed as a standard SOCP problem. It can be solved efficiently with complexity $O((NL)^{3.5} + J_f J_\phi (NL)^{2.5})$ using an optimization toolbox such as CVX [20], where J_f and J_ϕ are the total numbers of the discretization points in $f \in [f_L, f_U]$ and $\phi \in [-\pi,\pi]$, respectively.

Similarly, the coefficients of the compensation filter $\bar{H}_p(f)$ in (12), $p = -P,\ldots,P$, can be designed by solving the following problem

$$\min_{\bar{h}_{p,l}} \left\| \sum_{l=1}^{\bar{L}} \bar{h}_{p,l} \exp[-j2\pi(l-1)f/f_s] - B_p^{-1}(f) \right\|_2 \quad \text{for} \quad f \in [f_L, f_U] \tag{19}$$

where $\bar{h}_{p,l}$ is the lth filter coefficient of the pth phase mode and $\bar{L}$ is the number of filter taps. The above problem can again be reformulated in matrix form as

$$\begin{aligned} &\min_{\bar{\mathbf{h}}_p,\varepsilon} \varepsilon \\ &\text{s.t.} \quad \|\bar{\mathbf{c}}^T(f)\bar{\mathbf{h}}_p - B_p^{-1}(f)\|_2 \le \varepsilon \\ &\qquad f \in [f_L, f_U] \end{aligned} \tag{20}$$

where $\bar{\mathbf{h}}_p = [\bar{h}_{p,1},\ldots,\bar{h}_{p,\bar{L}}]^T$ and $\bar{\mathbf{c}}(f) = \{1, e^{-j2\pi f/f_s},\ldots, \exp[-j2\pi(\bar{L}-1)f/f_s]\}^T$. Likewise, by discretizing the constraints densely in $f \in [f_L, f_U]$, the complexity of solving the SOCP problem in (20) is $O(\bar{L}^{3.5} + J_f\bar{L}^{2.5})$.

Since filter coefficients with large amplitudes may lead to sensor noise amplification, the performance of the designed FIB in DOA estimation and adaptive beamforming may be considerably degraded. To address this problem we propose imposing norm constraints on the filter coefficients so as to limit the white-noise gain. Consequently, the problems (18) and (20) are, respectively, modified to

$$\begin{aligned} &\min_{\mathbf{h}_m,\varepsilon} \varepsilon \\ &\text{s.t.} \quad \|\mathbf{c}_m^T(f,\phi)\mathbf{h}_m - g_m(f,\phi)\|_2 \le \varepsilon \\ &\qquad \|\mathbf{h}_m\|_2 \le \eta, \quad \phi \in [-\pi,\pi], \quad f \in [f_L, f_U] \end{aligned} \tag{21}$$

and

$$\begin{aligned} &\min_{\bar{\mathbf{h}}_p,\varepsilon} \varepsilon \\ &\text{s.t.} \quad \|\bar{\mathbf{c}}^T(f)\bar{\mathbf{h}}_p - B_p^{-1}(f)\|_2 \le \varepsilon \\ &\qquad \|\bar{\mathbf{h}}_p\|_2 \le \xi, \quad f \in [f_L, f_U] \end{aligned} \tag{22}$$

where η and ξ are the upper bounds of the norms of the coefficient vectors, and they can be chosen according to the specification at hand. As shown by the design examples in Section V, the norm constraints can effectively prevent the noise from amplifying. For the sake of presentation, the proposed FIB that uses (18) and (20) is referred to as the unconstrained-FIB, whereas the one that uses (21) and (22) is referred to as the constrained-FIB.

IV. DESIGN OF UCCA-FIB WITH ELEVATION CONTROL

In previous sections we mainly focused on the design of UCCA-FIBs at the horizontal plane. In this section we show that the proposed method can be extended to provide an FI characteristic within a limited elevation range around the horizontal plane.

To start with let the desired elevation region be $\Theta = [\theta_L, \theta_U]$, where θ_L and θ_U are the lower and upper bounds of the region, respectively. The desired element pattern of the virtual UCA is denoted by $G(\theta, \phi)$, which is given according to the target applications. For simplicity the desired element pattern is assumed to be separable, and hence, it can be written as $G(\theta, \phi) = G_E(\theta)G_A(\phi)$, where $G_E(\theta)$ and $G_A(\phi)$ denote the elevation and azimuth patterns, respectively. Moreover, we assume that the azimuth pattern $G_A(\phi)$ of the virtual UCA is a periodic function, with period 2π as defined in (6). For simplicity the desired mth element response of the virtual UCA around the horizontal plane is chosen as $G(\theta, \phi - \varphi_m)\exp[j\beta r_V \cos(\phi - \varphi_m)]$ so that similar design procedure in (4)–(14) can be directly applied by treating $G_E(\theta)$ as a constant. Then, with appropriate design of LABFs, the mth element response of the virtual UCA is approximately given by

$$G_m(f, \theta, \phi) \approx G_E(\theta)G_A(\phi - \varphi_m)\exp[j\beta r_V \cos(\phi - \varphi_m)] \tag{23}$$

and the pth phase model of the virtual UCA is

$$\tilde{G}_p(f, \theta, \phi) \approx B_p(f)G_E(\theta)e^{jp\phi}. \tag{24}$$

Moreover, the spatial response of the final beamformer is $F(\theta, \phi) = \mathbf{w}^T\mathbf{a}_{PM}(\theta, \phi) = G_E(\theta)\sum_{p=-P}^{P} \cdot w_p e^{jp\phi}$, where $\mathbf{a}_{PM}(\theta, \phi) = [G_E(\theta)e^{-jP\phi}, G_E(\theta)e^{-j(P-1)\phi}, \ldots, G_E(\theta)e^{jP\phi}]^T$.

To obtain $G_m(f, \theta, \phi)$ in (23), the design problem of the LABF $H_n^{(m)}(f)$ is modified to (c.f. (18))

$$\begin{aligned} &\min_{\mathbf{h}_m, \varepsilon} \varepsilon \\ &\text{s.t.} \quad \|\mathbf{c}_m^T(f, \theta, \phi)\mathbf{h}_m - g_m(f, \theta, \phi)\|_2 \le \varepsilon, \\ &\qquad \phi \in [-\pi, \pi], \quad \theta \in [\theta_L, \theta_U], \quad f \in [f_L, f_U] \end{aligned} \tag{25}$$

where $\mathbf{h}_m$ and $\mathbf{c}_m(f, \theta, \phi)$ are defined as in (18) except that $\bar{E}_{n,l}^{(m)} = E_n^{(m)}(\theta, \phi - \varphi_m)\exp[j(\beta r_n \sin\theta\cos(\phi - \varphi_m) - 2\pi(l-1)f/f_s)]$ and $g_m(f, \theta, \phi) = G(\theta, \phi - \varphi_m) \cdot \exp[j\beta r_V \cos(\phi - \varphi_m)]$. If noise amplification is a problem, an additional norm constraint $\|\mathbf{h}_m\|_2 \le \eta$ can be imposed. Furthermore, from (24), we see that the design of compensation filter $\bar{H}_p(f)$ will not be influenced by the elevation pattern because of the separable phase model response. Hence, the methods developed in Section III for designing these filters can be directly adopted. Simulation results presented in Section VI show that this proposed method performs well and that FI characteristic in a prescribed elevation region around the horizontal plane can also be accomplished.

It is worth noting that the elevation control here utilizes the directivity of the sensor elements, and hence, only a limited elevation region can be controlled. It has been shown in [21]–[23] that arrays with elements placed in the elevation direction, e.g., uniform concentric spherical arrays, can be utilized to achieve full elevation control. Interested readers are referred to [21]–[23] and to the references therein.

V. DOA ESTIMATION AND ADAPTIVE BEAMFORMING

In this section the UCCA-FIB designed previously is employed for broadband DOA estimation and adaptive beamforming. For the sake of simplicity, we only consider the plane at $\theta = \pi/2$ here. Assuming that D broadband signals impinge on the UCCA at angles $\Phi = \{\phi_1, \phi_2, \ldots, \phi_D\}$, respectively, the output signal at each element of the array can be written as

$$x_n^{(m)}[t, \Phi] = \sum_{i=1}^{D} s_i[t - \tau_n^{(m)}(\phi_i)] + v_n^{(m)}[t] \tag{26}$$

where $n = 1, \ldots, N$, $m = 1, \ldots, M$, $s_i[t]$ is the ith signal that impinges the array at angle ϕ_i and $\tau_n^{(m)}(\phi_i) = r_n\cos(\phi_i - \varphi_m)/c$ denotes the propagation delay to the nth element of the mth linear array associated with the ith source. $v_n^{(m)}[t]$ is the additive white Gaussian noise at the nth element of the mth linear array. Hence, the vector $\mathbf{x}_m[t, \Phi] = [x_1^{(m)}[t, \Phi], x_2^{(m)}[t, \Phi], \ldots, x_N^{(m)}[t, \Phi]]^T$ is the snapshot of the mth linear array at sampling instance t. The frequency response of the array output $\mathbf{x}_m[t, \Phi]$ can be written as

$$\mathbf{X}_m(f, \Phi) = \mathbf{A}_m(f, \Phi)\mathbf{S}(f) + \mathbf{V}_m(f) \tag{27}$$

where $\mathbf{A}_m(f, \Phi) = [\mathbf{a}^{(m)}(f, \phi_1), \ldots, \mathbf{a}^{(m)}(f, \phi_D)]$ is the $N \times D$ source direction matrix for the mth linear array, $\mathbf{a}^{(m)}(f, \phi_i)$, $i = 1, \ldots, D$, is the steering vector of the mth linear array that corresponds to the ith signal, $\mathbf{S}(f) = [S_1(f), \ldots, S_D(f)]^T$ is the $D \times 1$ source signal spectrum vector, and $\mathbf{V}_m(f) = [V_1^{(m)}(f), \ldots, V_N^{(m)}(f)]^T$ is the frequency response of the sensor noise vector of the mth linear array. Each output $X_n^{(m)}, (f, \Phi)$ is first filtered by the LABF $H_n(f)$, and the N outputs are

summed to obtain the output of the mth element of the virtual UCA

$$\begin{aligned} Y_m(f,\Phi) &= \mathbf{H}_m^T(f)\mathbf{X}_m(f,\Phi) \\ &= \mathbf{H}_m^T(f)\mathbf{A}_m(f,\Phi)\mathbf{S}(f) + \mathbf{H}_m^T(f)\mathbf{V}_m(f) \\ &= \bar{\mathbf{A}}_m^T(f,\Phi)\mathbf{S}(f) + \bar{V}_m(f) \end{aligned} \tag{28}$$

where the mth LABF $\mathbf{H}_m(f) = [H_1^{(m)}(f),\ldots,H_N^{(m)}(f)]^T$ is designed to satisfy (4) using SOCP, as described in Section III

$$\begin{aligned} \bar{\mathbf{A}}_m(f,\Phi) &= \mathbf{H}^T(f)\mathbf{A}_m(f,\Phi) \\ &\approx \{G(\phi_1-\varphi_m)\exp[j\beta r_V\cos(\phi_1-\varphi_m)],\ldots, \\ &\quad G(\phi_D-\varphi_m)\exp[j\beta r_V\cos(\phi_D-\varphi_m)]\}^T \end{aligned}$$

and $\bar{V}_m(f) = \mathbf{H}_m^T(f)\mathbf{V}_m(f)$. Consequently, the frequency response of the virtual UCA outputs $\mathbf{Y}(f,\Phi) = [Y_1(f,\Phi),\ldots,Y_M(f,\Phi)]^T$ can be rewritten more compactly in matrix form as

$$\mathbf{Y}(f,\Phi) = \bar{\mathbf{A}}(f,\Phi)\mathbf{S}(f) + \bar{\mathbf{V}}(f) \tag{29}$$

where

$$\begin{aligned} \bar{\mathbf{A}}(f,\Phi) &= [\bar{\mathbf{A}}_1(f,\Phi),\ldots,\bar{\mathbf{A}}_M(f,\Phi)]^T \\ &= [\mathbf{a}_V(f,\phi_1),\ldots,\mathbf{a}_V(f,\phi_D)] \end{aligned}$$

is the steering matrix of the virtual UCA and $\bar{\mathbf{V}}(f) = [\bar{V}_1(f),\ldots,\bar{V}_M(f)]^T$ denotes the frequency response of the additive noise vector. After transforming (29) to phase modes by IDFT, the output of the pth phase mode becomes

$$\begin{aligned} Z_p(f,\Phi) &= \mathbf{W}_p^T\mathbf{Y}(f,\Phi) \\ &= \mathbf{W}_p^T\bar{\mathbf{A}}(f,\Phi)\mathbf{S}(f) + Q_p(f) \end{aligned} \tag{30}$$

where $\mathbf{W}_p = M^{-1}[e^{jp\varphi_1},e^{jp\varphi_2},\ldots,e^{jp\varphi_M}]^T$ and $Q_p(f) = \mathbf{W}_p^T\bar{\mathbf{V}}(f)$ is the noise of the pth phase mode. Moreover, according to (5)–(9), it is known that

$$\begin{aligned} \mathbf{W}_p^T\bar{\mathbf{A}}(f,\Phi) &= \mathbf{W}_p^T[\mathbf{a}_V(f,\phi_1),\ldots,\mathbf{a}_V(f,\phi_D)] \\ &\approx B_p(f)[e^{jp\phi_1},\ldots,e^{jp\phi_D}]. \end{aligned} \tag{31}$$

To remove the frequency dependency, each phase mode, i.e., $Z_p(f,\Phi)$, should be filtered by $\bar{H}_p(f)$, which should be designed to approximate $B_p^{-1}(f)$ by using SOCP. Therefore, one gets the compensated output as

$$\begin{aligned} \bar{Z}_p(f,\Phi) &= \bar{H}_p(f)Z_p(f,\Phi) \\ &\approx B_p^{-1}(f)\mathbf{W}_p^T\mathbf{Y}(f,\Phi) \\ &= \sum_{i=1}^{D} e^{jp\phi_i}S_i(f) + B_p^{-1}(f)Q_p(f). \end{aligned} \tag{32}$$

The vector of these compensated phase modes can be written as

$$\begin{aligned} \bar{\mathbf{Z}}(f,\Phi) &= [\bar{Z}_{-P}(f,\Phi),\bar{Z}_{-(P-1)}(f,\Phi),\ldots,\bar{Z}_P(f,\Phi)]^T \\ &= \mathbf{A}_{PM}(\Phi)\mathbf{S}(f) + \bar{\mathbf{Q}}(f) \end{aligned} \tag{33}$$

where $\mathbf{A}_{PM}(\Phi) = [\mathbf{a}_{PM}(\phi_1),\ldots,\mathbf{a}_{PM}(\phi_D)]$ and $\bar{\mathbf{Q}}(f) = [B_{-P}^{-1}(f)Q_{-P}(f),B_{-(P-1)}^{-1}(f)Q_{-(P-1)}(f),\ldots,B_P^{-1}(f)\cdot Q_P(f)]^T$. Finally, by taking the inverse Fourier transform (FT) of (33), the output of the virtual UCA in time domain becomes

$$\bar{\mathbf{z}}[t,\Phi] \approx \mathbf{A}_{PM}(\Phi)\mathbf{s}[t] + \bar{\mathbf{q}}[t]. \tag{34}$$

It can be seen that the outputs of the UCCA are first transformed by LABF $\mathbf{H}_m(f)$ to those of a virtual UCA. Moreover, the frequency dependency in the frequency band of interest is compensated by the proposed FIB network. The resultant outputs fall into the form of ULAs, as shown in (34). Hence, conventional methods of DOA estimation and beamforming for narrowband signals can be directly applied.

We now proceed to estimate the DOAs by using the conventional MUSIC algorithm based on the output $\bar{\mathbf{z}}[t,\Phi]$. First, we note that the covariance matrix of the output is

$$\mathbf{R}_{\bar{z}} = E\{\bar{\mathbf{z}}[t,\Phi]\bar{\mathbf{z}}^H[t,\Phi]\} = \mathbf{A}_{PM}(\Phi)\mathbf{R}_s\mathbf{A}_{PM}^H(\Phi) + \mathbf{R}_{\bar{q}} \tag{35}$$

where $E\{\cdot\}$ denotes mathematical expectation. $\mathbf{R}_s = E\{\mathbf{s}[t]\mathbf{s}^H[t]\}$ is the signal covariance matrix, and $\mathbf{R}_{\bar{q}} = E\{\bar{\mathbf{q}}[t]\bar{\mathbf{q}}^H[t]\}$ is the noise covariance matrix. In the finite sample case, $\mathbf{R}_{\bar{z}}$ can be estimated as

$$\hat{\mathbf{R}}_{\bar{z}} = \frac{1}{T}\sum_{t=1}^{T}\bar{\mathbf{z}}[t,\Phi]\bar{\mathbf{z}}^H[t,\Phi] \tag{36}$$

where T is the total number of snapshots.

In order to estimate the DOAs, we denote the eigendecomposition of $(\mathbf{R}_{\bar{z}},\mathbf{R}_{\bar{q}})$ as $\mathbf{R}_{\bar{z}}\mathbf{E} = \Lambda\mathbf{R}_{\bar{q}}\mathbf{E}$, where Λ is a diagonal matrix of sorted eigenvalues $\mathbf{E} = [\mathbf{E}_S \mid \mathbf{E}_N]$, and $\mathbf{E}_S$ and $\mathbf{E}_N$ are the eigenvectors of the signal and noise subspaces, respectively. Then, similar to the conventional MUSIC algorithm, the source directions can be determined by searching for the D peak positions of the following spatial spectrum

$$P_{\text{FIB-MUSIC}}(\phi) = \frac{\mathbf{a}_{PM}^H(\phi)\mathbf{a}_{PM}(\phi)}{\mathbf{a}_{PM}^H(\phi)\mathbf{E}_N\mathbf{E}_N^H\mathbf{a}_{PM}(\phi)}. \tag{37}$$

Furthermore, broadband beamforming can be performed to enhance the signal at a desired angle, say ϕ_d. The conventional beamforming techniques such as the minimum variance distortionless response (MVDR) beamforming can be employed to suppress the interferences. The resultant beamformer weight

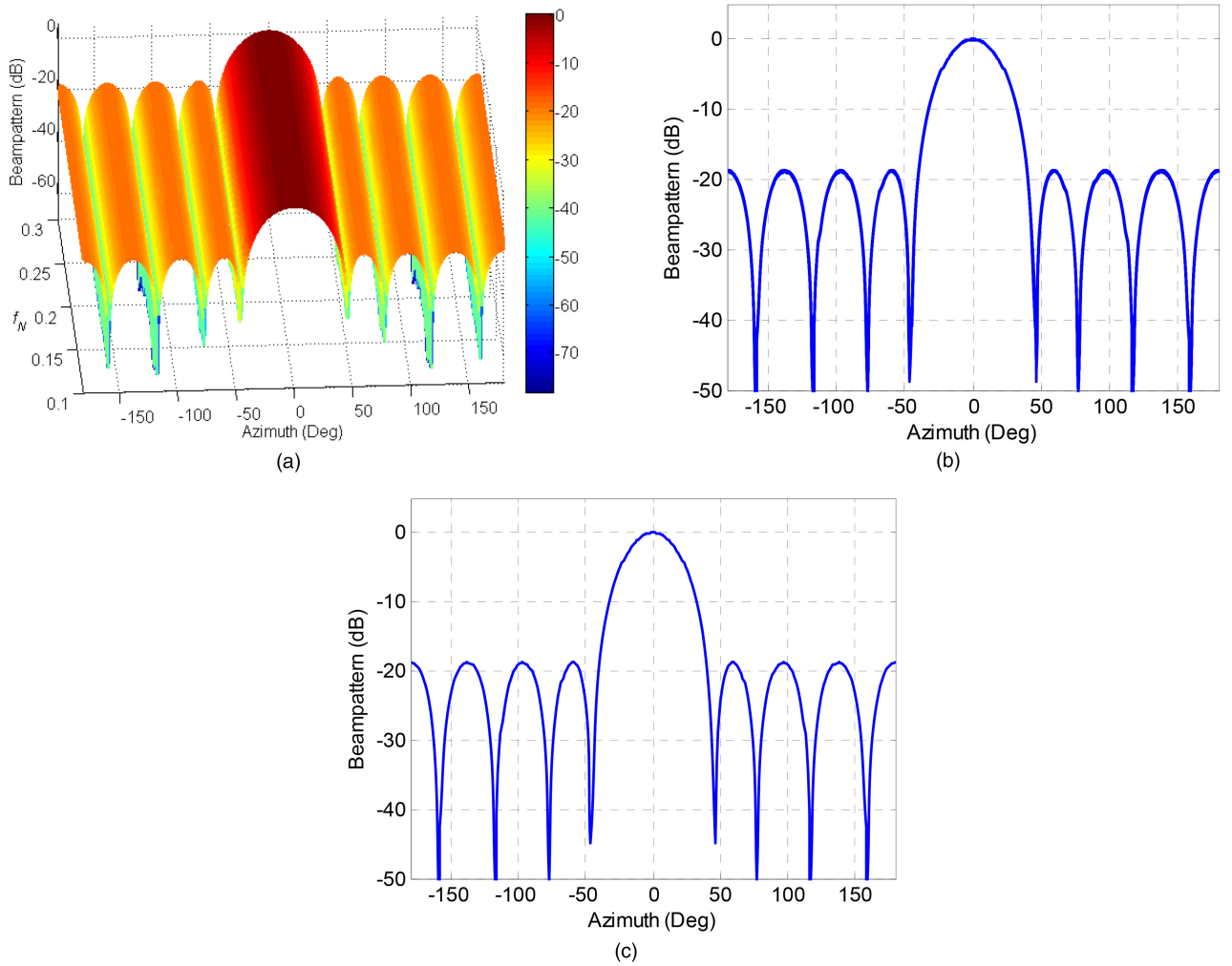

Fig. 3. (a) Spatial-frequency response of proposed unconstrained-FIB with omnidirectional elements (example 1). (b) Beampatterns of proposed unconstrained-FIB over normalized frequency $f_N \in [0.1, 0.3]$ with omnidirectional elements (example 1). (c) Desired beampattern with omnidirectional elements (example 1).

vector of the MVDR is

$$\mathbf{w}_{\text{FIB-MVDR}} = \frac{\hat{\mathbf{R}}_{\bar{z}}^{-1}\mathbf{a}_{PM}(\phi_d)}{\mathbf{a}_{PM}^H(\phi_d)\hat{\mathbf{R}}_{\bar{z}}^{-1}\mathbf{a}_{PM}(\phi_d)}. \tag{38}$$

From the simulation results presented in the next section, broadband interferences can be successfully suppressed using the designed FIB and MVDR beamformer in (38).

VI. DESIGN EXAMPLES AND SIMULATION RESULTS

In this section a six-ring UCCA is considered. Each ring is composed of 20 elements. Moreover, each linear subarray of the UCCA is assumed to be a ULA with an inter-element spacing of $d = \lambda_{\min}/4$, where $\lambda_{\min} = c/f_U$ is the minimal wavelength of the signals. The frequency band of interest of the UCCA-FIB is assumed to be $f_N \in [f_L, f_U]/f_s = [0.1, 0.3]$, which is normalized by the sampling frequency f_s. The radius of each ring is assumed to be $r_n = (n+4)d$, and the virtual radius is set to be $r_V = 6d$. From our simulation results in example 2 presented later, it should be found that r_V should be chosen in the range $[r_1, r_N]$, which, in this example, is equal to $[5d, 10d]$. In all simulations the number of filter coefficients is $L = \bar{L} = 20$, and the number of phase modes is chosen to be nine. The element pattern of the virtual UCA considered is $G(\phi) = 1 + \cos\phi$, except example 3. The beamforming weight vector $\mathbf{w}$ for the desired beampattern is obtained using the CFIRPM command in Matlab.

EXAMPLE 1 UCCA with Omnidirectional Elements In this example we illustrate the FI characteristic of the proposed UCCA-FIB with omnidirectional elements by designing a beampattern with the main beam targeted at 0°. The resultant spatial response of the designed unconstrained-FIB based on (18) and (20) is shown in Fig. 3(a). Moreover, the spatial responses for 21 uniformly spaced frequency points in $f_N \in [0.1, 0.3]$ are plotted together in Fig. 3(b) to illustrate the FI property of the FIB. It can be seen that the frequency spectrum is approximately invariant over the desired bandwidth and that it is

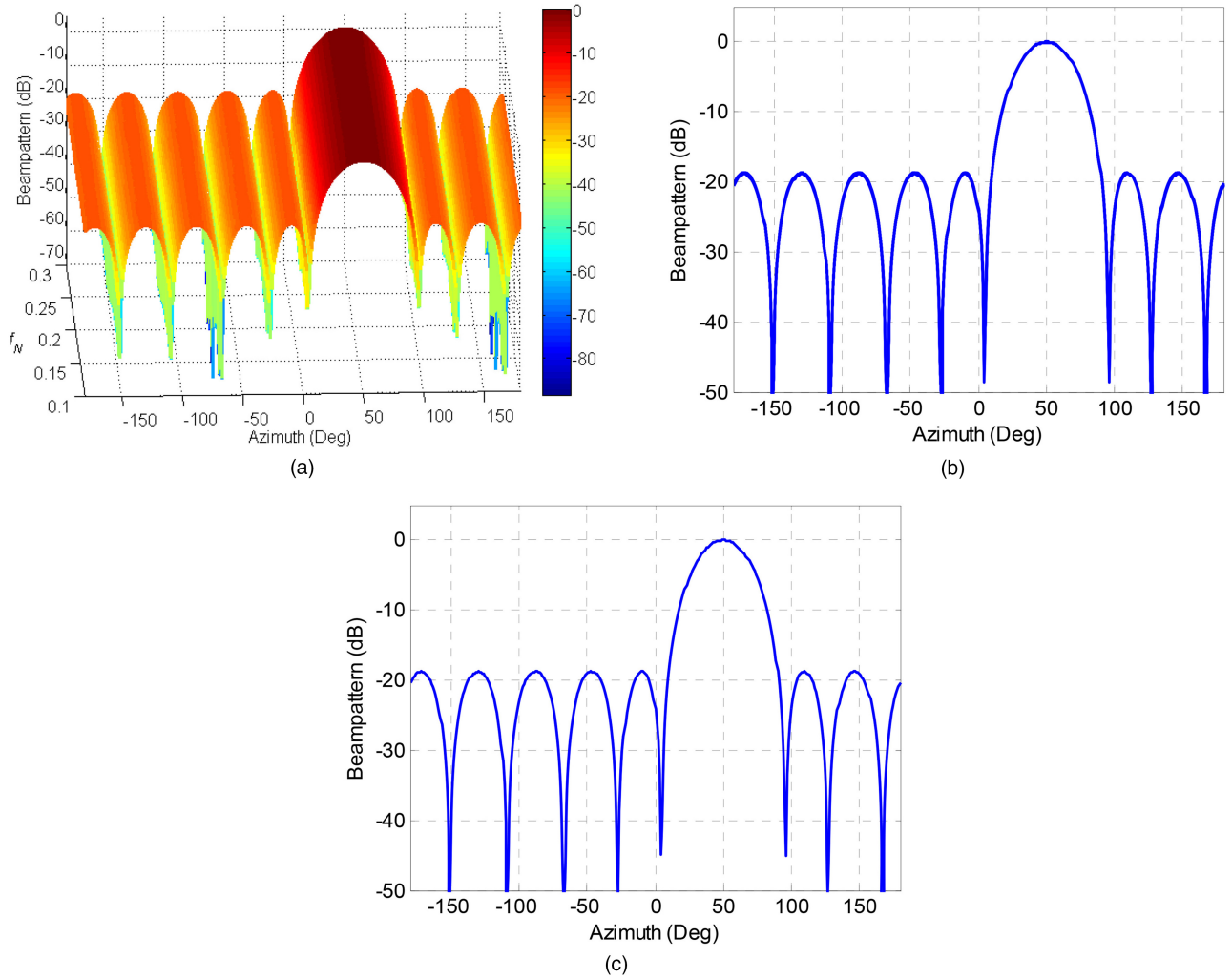

Fig. 4. (a) Spatial-frequency response of proposed unconstrained-FIB with directional elements (example 2). (b) Beampatterns of proposed unconstrained-FIB over normalized frequency $f_N \in [0.1, 0.3]$ with directional elements (example 2). (c) Desired beampattern with directional elements (example 2).

nearly identical to the desired beampattern as shown in Fig. 3(c).

EXAMPLE 2 UCCA with Directional Elements Instead of omnidirectional elements we proceed to illustrate the FI characteristic of the proposed UCCA-FIB with directional elements in this example, and the main beam of the desired beampattern is targeted at 50°. For illustration purposes we assume that the element pattern of each sensor element is $E_n^{(m)}(\phi) = 1 + 0.5\cos^{n-1}(\phi)$, $n = 1, \ldots, N$ and, hence, that each ring is composed of identical sensor elements. Figures 4(a) and (b) show the resultant beampatterns of the proposed unconstrained-FIB. It can be seen that the frequency spectrum is approximately invariant over the desired bandwidth, even though the elements are directional. Moreover, the frequency spectrum is approximately identical to the desired one shown in Fig. 4(c). Comparing the proposed method with results shown in Example 1, it is found that the proposed method still performs quite well in the case of directional elements. We now test the performance of the proposed constrained-FIB based on (21) and (22). For illustration purposes we choose $\eta = 2$ and $\xi = 5$. Figures 5(a) and (b) show the spatial-frequency response of the proposed constrained-FIB with directional elements. We notice that the constrained-FIB still offers FI characteristic over the desired bandwidth. Comparing it with the unconstrained-FIB, the beampatterns exhibit slightly increased variations since the filter coefficients, and hence sensor noise amplification, are bounded by the norm constraints. Therefore, the bound values of η and ξ should be chosen to balance the beampattern variations and noise amplification. However, in practical applications, the constrained-FIB is preferred since its performance in DOA estimation and adaptive beamforming is much better than the unconstrained-FIB as we illustrate further in example 4.

In order to study the effect of the virtual radius r_V on the performance of the proposed FIB, Fig. 6 shows

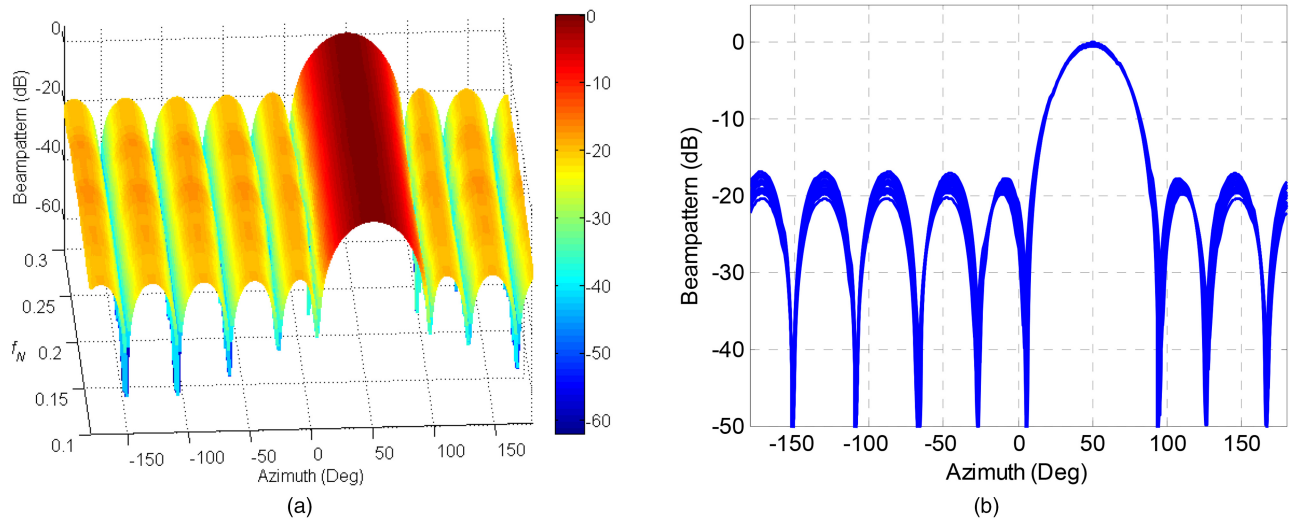

Fig. 5. (a) Spatial-frequency response of proposed constrained-FIB with directional elements, $\eta = 2$ and $\xi = 5$ (example 2). (b) Beampatterns of the proposed constrained-FIB over normalized frequency $f_N \in [0.1, 0.3]$ with directional elements, $\eta = 2$ and $\xi = 5$ (example 2).

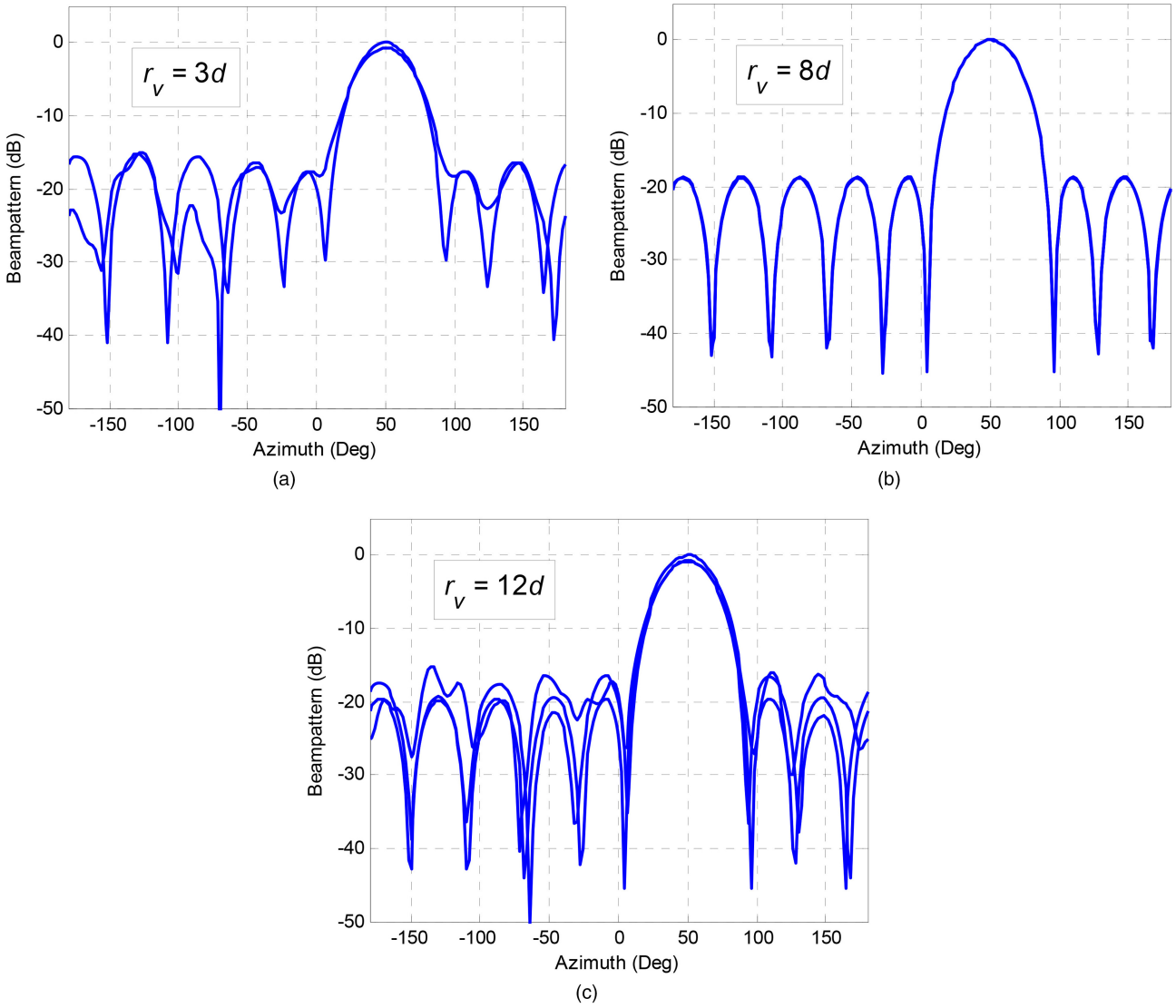

Fig. 6. Beampatterns with different virtual radius r_V (only response of $f_N = 0.1$, 0.2, and 0.3 are shown in each figure). (a) $r_V = 3d$. (b) $r_V = 8d$. (c) $r_V = 12d$ (example 2).

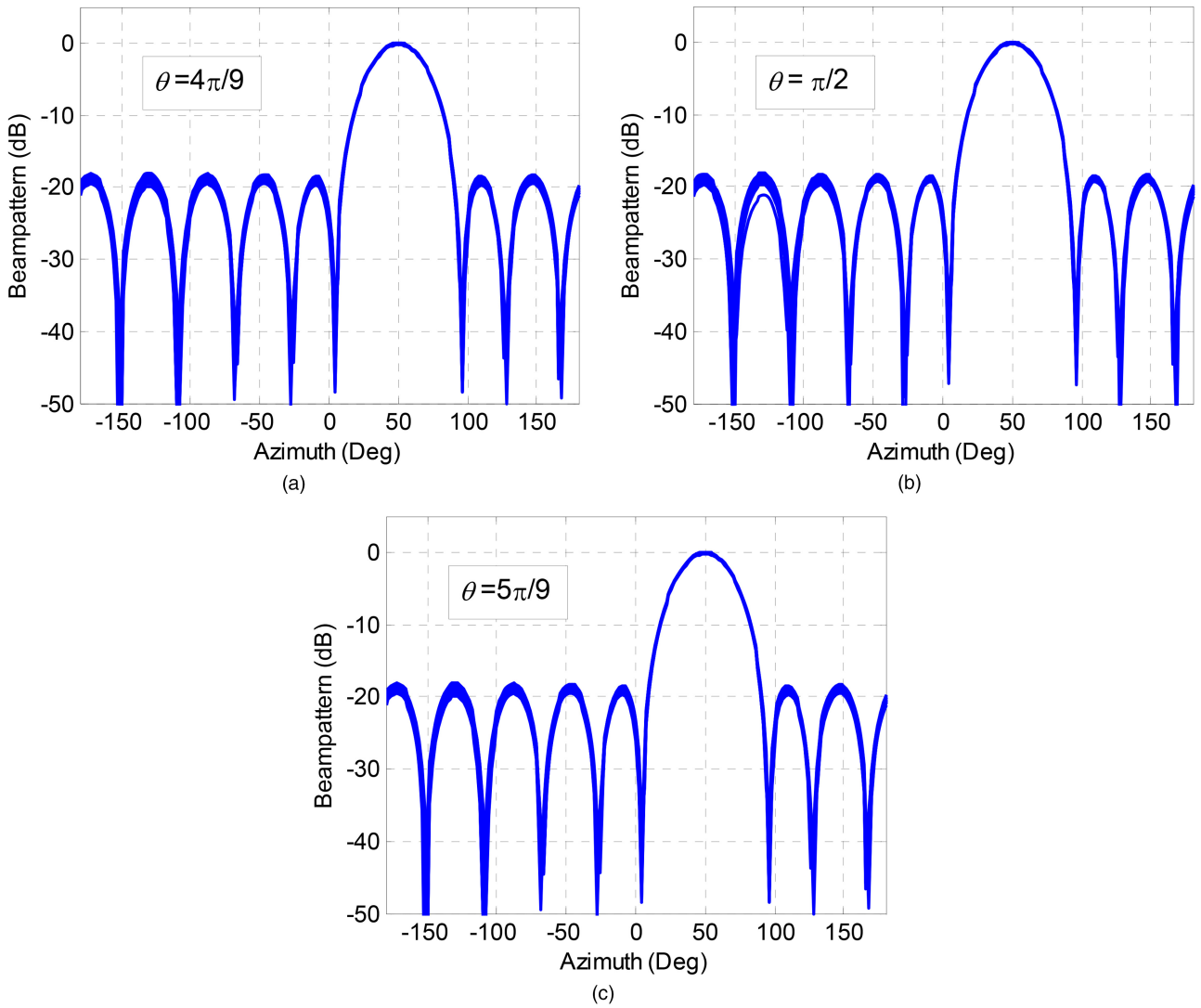

Fig. 7. Beampatterns at different elevation angles over normalized frequency $f_N \in [0.1, 0.3]$. (a) $\theta = 80°$. (b) $\theta = 85°$. (c) $\theta = 90°$ (example 3).

the beampatterns designed with different values of r_V. It can be found experimentally that the performance may degrade significantly when r_V is outside the range $[r_1, r_N]$. When r_V is chosen in this range, the obtained and desired (ideal) beampatterns are nearly identical. This suggests that the desired pattern of each linear array can be obtained by choosing a radius r_V within the range $[r_1, r_N]$, otherwise, performance degradation may be experienced.

EXAMPLE 3 Elevation Control To illustrate the capability of the proposed method of offering FI characteristics at elevation angles around the horizontal plane, we follow the array settings given in example 2 and assume that the element pattern of each sensor element is $E_n^{(m)}(\theta, \phi) = 1 + \sin\theta \cos^{n-1}\phi$, $n = 1, \ldots, N$ and that the desired element pattern of the virtual UCA is $G(\theta, \phi) = G_E(\theta) G_A(\phi) = \sin\theta(1 + \cos\phi)$. The elevation region to be controlled is $[\theta_L, \theta_U] = [4\pi/9, 5\pi/9]$. Figure 7 depicts the beampatterns at different elevation angles using the proposed nconstrained-FIB. It can be seen that the response within the prescribed elevation region is approximately FI. The results demonstrate that the proposed method can be utilized to control the elevation spatial pattern around the horizontal plane. However, as discussed in Section IV, the FI property will be degraded for larger elevation angles since only a limited elevation region can be controlled due the limitation of the array geometry.

EXAMPLE 4 Broadband DOA Estimation and Beamforming In this example the effectiveness of the proposed FIB for broadband DOA estimation and beamforming is evaluated using the UCCA with directional elements described in example 2. For comparison we apply the proposed method with norm constraint to a UCA with element pattern $1 + \cos\phi$ directly. First, the performance of the proposed FIBs for DOA estimation is tested. Two broadband

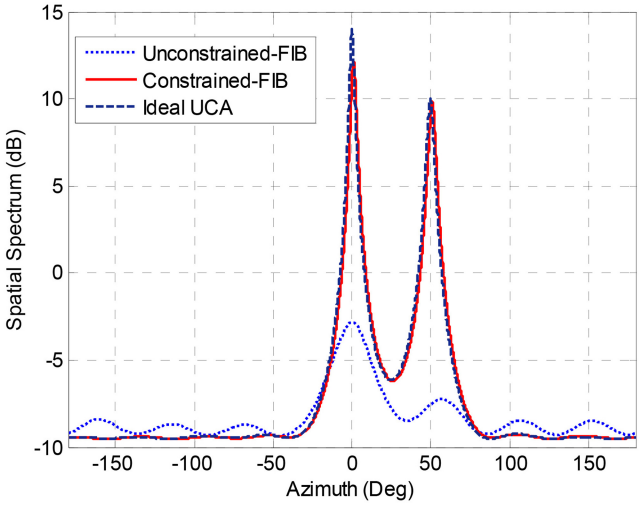

Fig. 8. Spatial spectra using phase model based MUSIC algorithm, $\eta = 2$ and $\xi = 5$ (example 4).

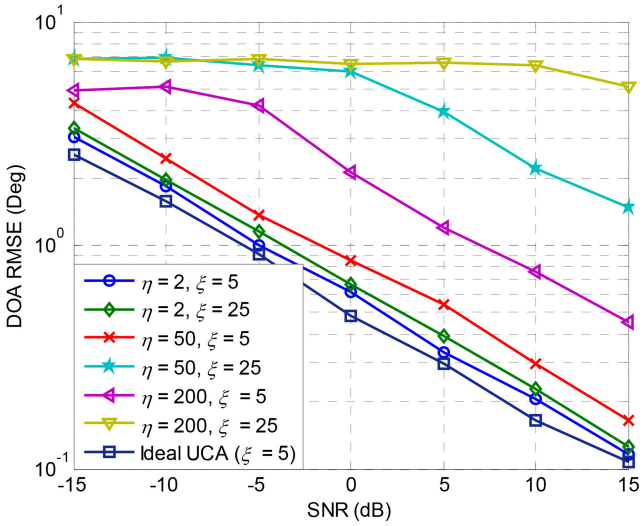

Fig. 9. RMSEs of DOA estimation using constrained-FIB with different filter coefficient vector bounds (example 4).

incoherent signals with equal power impinge on the array from angles $\phi_1 = 0°$ and $\phi_2 = 50°$, respectively. The normalized bandwidth of the signals is assumed to be [0.1,0.15] and [0.2,0.25], respectively. Let the signal-to-noise ratio (SNR) be 0 dB. Figure 8 shows the MUSIC spatial spectrum computed by (37) for DOA estimation using the proposed FIBs. It can be seen that the unconstrained-FIBs just marginally resolve the two DOAs due to the fact that the noise is considerably amplified by the FIB networking with large filter coefficients. On the other hand the DOAs can be correctly estimated using the constrained-FIB since the noise is well controlled by restricting the filter coefficients. The reason is that the noise is considerably amplified by the FIB networking with large filter coefficients, and hence, the SNR is this case is significantly reduced. However, since the filter coefficients are bounded

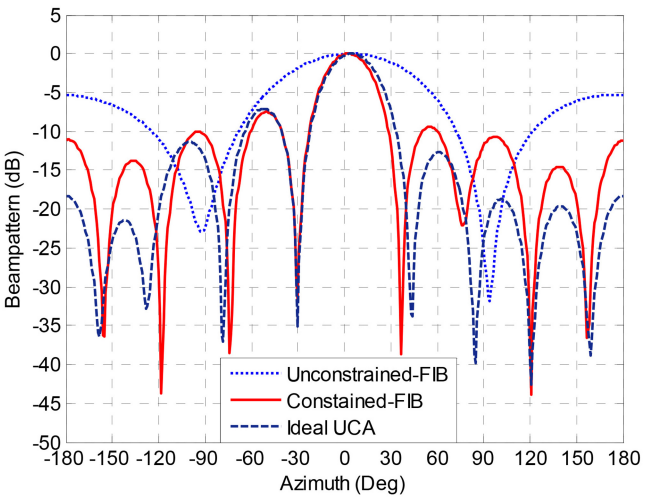

Fig. 10. Response of MVDR beamformer, desire signal $\phi_d = 0°$, interferences $\phi_1 = -30°$, $\phi_2 = 120°$, $\eta = 2$ and $\xi = 5$ (example 4).

as in (21) and (22), the noise amplification can be effectively suppressed. Figure 9 shows the root mean square error (RMSE) of estimating the DOA of the two broadband signals versus input SNRs using the proposed constrained-FIB with different filter coefficient bounds. The result at each SNR is obtained from 200 independent simulations. We can notice that for small bounds, the proposed constrained-FIB can offer quite good performance even at lower SNR levels, whereas when the bounds become larger, the performance tends to degrade. We now test the effectiveness of the proposed constrained-FIB for broadband beamforming. More precisely the desired signal is assumed to impinge on the array at an angle of 0°, while two interferences are from angles of $-30°$ and 120°. The SNR of the desired signal is 0 dB, and the SNRs of the interferences are 30 dB. The beamforming weight vector is obtained using the MVDR algorithm as shown in (38), and the resultant spatial response for interference rejection is shown in Fig. 10. It can be seen that the interferences can be successfully suppressed with the proposed constrained-FIB using the MVDR beamformer in (38). However, the interferences are not completely rejected by the unconstrained-FIB due to the amplification of noise. Finally, it can be noticed from Figs. 8–10 that our proposed method with norm constraints that use UCCAs can offer comparable performance to the FI UCAs with ideal element pattern $1 + \cos\phi$.

VII. CONCLUSIONS

A new, decoupled approach for designing FI UCCAs with directional elements and its applications to DOA estimation and adaptive beamforming have been presented. By using appropriately designed beamformers, each subarray along the radial direction of the UCCA is transformed to an element with appropriate directivity. Consequently, the whole UCCA can be viewed as a virtual UCA with a desired

directivity element pattern. By extending the approach for designing FI-UCAs, the frequency dependency of the virtual UCA is compensated to facilitate broadband DOA and adaptive beamforming. The LABFs and compensation filters can be designed separately, and the problems are formulated as SOCP programming problems, which can be solved optimally and efficiently. Additional norm constraints on the coefficients of the LABFs and compensation filters are also incorporated to address the possible noise amplification problem in large UCCAs. Numerical examples are provided to demonstrate the effectiveness and improvement of the proposed methods in DOA estimation, adaptive beamforming, and elevation control over the conventional FI-UCCA design method.

REFERENCES

[1] Krim, H. and Viberg, M.
Two decades of array signal processing research: The parametric approach.
IEEE Signal Processing Magazine, **13** (July 1996), 67–94.

[2] Liu, W. and Weiss, W.
Wideband Beamforming: Concepts and Techniques.
Hoboken, NJ: Wiley, Mar. 2010.

[3] Liu, W. and Langley, R. J.
An adaptive wideband beamforming structure with combined subband decomposition.
IEEE Transactions on Antennas and Propagation, **57** (July 2009), 2204–2207.

[4] Liu, W., Weiss, S., and Hanzo, L.
A subband-selective broadband GSC with cosine-modulated blocking matrix.
IEEE Transactions on Antennas and Propagation, **52** (Mar. 2004), 813–820.

[5] Liu, W. and Weiss, S.
Design of frequency invariant beamformers for broadband arrays.
IEEE Transactions on Signal Processing, **56** (Feb. 2008), 855–860.

[6] Ward, D. B., Kennedy, R. A., and Williamson, R. C.
Theory and design of broadband sensor arrays with frequency invariant far-field beam patterns.
Journal of the Acoustical Society of America, **97** (Feb. 1995), 1023–1034.

[7] Ward, D. B., Kennedy, R. A., and Williamson, R. C.
FIR filter design for frequency invariant beamformers.
IEEE Signal Processing Letters, **3** (Mar. 1996), 69–71.

[8] Ward, D. B., Ding, Z., and Kennedy, R. A.
Broadband DOA estimation using frequency invariant beamforming.
IEEE Transactions on Signal Processing, **46** (May 1998), 1463–1469.

[9] Nishikawa, K., et al.
Wideband beamforming using fan filter.
Proceedings of the IEEE International Symposium on Circuits and Systems (IEEE ISCAS), vol. 2, San Diego, CA, May 10–13, 1992, pp. 533–536.

[10] Sekiguchi, T. and Karasawa, Y.
Wideband beamspace adaptive array utilizing FIR fan filters for multibeam forming.
IEEE Transactions on Signal Processing, **48**, 1 (Jan. 2000), 277–284.

[11] Chan, S. C. and Pun, C. K. S.
On the design of digital broadband beamformer for uniform circular array with frequency invariant characteristics.
Proceedings of the IEEE International Symposium on Circuits and Systems (ISCAS 2002), vol. 1, Scottsdale, AZ, May 26–29, 2002, pp. 693–696.

[12] Yang, Y., Sun, C., and Wan, C.
Theoretical and experimental studies on broadband constant beamwidth beamforming for circular arrays.
Proceedings of OCEANS 2003, vol. 3, San Diego, CA, Sept. 22–26, 2003, pp. 1647–1653.

[13] Chan, S. C. and Chen, H. H.
Theory and design of uniform concentric circular arrays with frequency invariant characteristics.
Proceedings of the IEEE International Conference on Acoustics, Speech, and Signal Processing (ICASSP), vol. 4, Philadelphia, PA, Mar. 18–23, 2005, pp. 805–808.

[14] Chan, S. C. and Chen, H. H.
Uniform concentric circular arrays with frequency-invariant characteristics—Theory, design, adaptive beamforming and DOA estimation.
IEEE Transactions on Signal Processing, **55** (Jan. 2007), 165–177.

[15] Chen, H. H., Chan, S. C., and Ho, K. L.
Adaptive beamforming using frequency invariant uniform concentric circular arrays.
IEEE Transactions on Circuits and Systems I: Regular Papers, **54**, 9 (Sept. 2007), 1938–1949.

[16] Davies, D. E. N.
Circular arrays.
In A. W. Rudge, K. Milne, A. D. Olver, and P. Knight (Eds.), *The Handbook of Antenna Design*, vol. 2, London: Peter Peregrinus Ltd., 1983.

[17] Rahim, T. and Davies, D. E. N.
Effect of directional elements on the directional response of circular antenna arrays.
IEE Proceedings—Part H: Microwaves, Optics and Antennas, **129**, 1 (Feb. 1982), 18–22.

[18] Rahim, T.
Analysis of the element pattern shape for circular arrays.
Electronics Letters, **19** (Sept. 1983), 838–840.

[19] Schmidt, R. O.
Multiple emitter location and signal parameter estimation.
IEEE Transactions on Antennas and Propagation, **AP-34** (Mar. 1986), 276–280.

[20] Grant, M. and Boyd, S.
CVX: Matlab software for disciplined convex programming.
Version 1.21, http://cvxr.com/cvx, May 2010.

[21] Chan, S. C. and Chen, H. H.
Theory and design of uniform concentric spherical arrays with frequency invariant characteristics.
Proceedings of the IEEE International Conference on Acoustics, Speech, and Signal Processing (ICASSP 2006), vol. 4, Toulouse, France, May 14–19, 2006, pp. 1057–1060.

[22] Chen, H. H. and Chan, S. C.
Adaptive beamforming and DOA estimation using uniform concentric spherical arrays with frequency invariant characteristics.
Journal of VLSI Signal Processing, **46** (2007), 15–34.

[23] Chen, H. H., et al.
Adaptive beamforming and recursive DOA estimation using frequency-invariant uniform concentric spherical arrays.
IEEE Transactions on Circuits and Systems I: Regular Papers, **55** (Nov. 2008), 3077–3089.

Bin Liao (S'09) received his B.Eng. and M.Eng. degrees from Xidian University, Xi'an, China, in 2006 and 2009, respectively. He is currently pursuing a Ph.D. in the Department of Electrical and Electronic Engineering at the University of Hong Kong.

His main research interests are array signal processing and adaptive filtering.

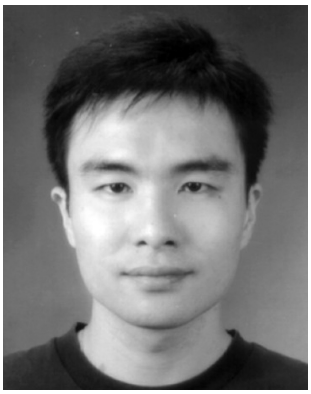

Kai-Man Tsui received his B.Eng., M.Phil., and Ph.D. degrees in electrical and electronic engineering from the University of Hong Kong, in 2001, 2004, and 2008, respectively.

He is currently working as a postdoctoral fellow in the Department of Electrical and Electronic Engineering at the University of Hong Kong. His main research interests are in array signal processing, high-speed AD converter architecture, biomedical signal processing, digital signal processing, multirate filter bank and wavelet design, and digital filter design, realization, and application.

Shing-Chow Chan (S'87—M'92) received his B.S. (Eng.) and Ph.D. degrees from the University of Hong Kong, in 1986 and 1992, respectively.

Since 1994 he has been with the University of Hong Kong and currently is an associate professor. He was a visiting researcher with the Microsoft Corporation, Redmond, WA and Microsoft, Beijing, China, in 1998 and 1999, respectively. His research interests include fast transform algorithms, filter design and realization, multirate signal processing, and imagebased rendering.

Dr. Chan is currently an Associate Editor of the *IEEE Transactions on Circuits and Systems—I: Regular Papers* and of the *Journal of Very Large Scale Integration Signal Processing and Video Technology*. He is also a member of the Digital Signal Processing Technical Committee of the IEEE Circuits and Systems Society. He was the Chairman of the IEEE Hong Kong Chapter of Signal Processing from 2000 to 2002.